

1 **Modelling changes in glutathione homeostasis as a function of quinone**

2 **redox metabolism**

3 Ross A. Kelly^a, Joseph Leedale^{b*}, Dominic Calleja^c, Steven J. Enoch^d, Andy Harrell^e, Amy E.

4 Chadwick^f and Steven Webb^a

5 ^a Department of Applied Mathematics, Liverpool John Moores University, Byrom Street,

6 Liverpool, L3 3AF, UK

7 ^b EPSRC Liverpool Centre for Mathematics in Healthcare, Department of Mathematical

8 Sciences, University of Liverpool, Liverpool, L69 7ZL, UK

9 ^c Institute for Risk and Uncertainty, University of Liverpool, Liverpool, L69 7ZF, UK

10 ^d School of Pharmacy and Biomolecular Sciences, Liverpool John Moores University, Byrom

11 Street, Liverpool, L3 3AF, UK

12 ^e GlaxoSmithKline, David Jack Centre for Research, Park Road, Ware, SG12 0DP, UK

13 ^f MRC Centre for Drug Safety Science, Department of Molecular and Clinical Pharmacology,

14 University of Liverpool, Ashton Street, Liverpool, L69 3GE, UK

15 * Corresponding author

16 Email: j.ledale@liverpool.ac.uk (JL)

17

18 **Abstract**

19 Redox cycling is an understated mechanism of toxicity associated with a plethora of
20 xenobiotics, responsible for preventing the effective treatment of serious conditions such as
21 malaria and cardiomyopathy. Quinone compounds are notorious redox cyclers, present in
22 drugs such as doxorubicin, which is used to treat a host of human cancers. However, the
23 therapeutic index of doxorubicin is undermined by dose-dependent cardiotoxicity, which may
24 be a function of futile redox cycling. In this study, a doxorubicin-specific *in silico* quinone
25 redox metabolism model is described. Doxorubicin-GSH adduct formation kinetics are

26 thermodynamically estimated from its reduction potential, while the remainder of the model
27 is parameterised using oxygen consumption rate data, indicative of hydroquinone auto-
28 oxidation. The model is then combined with a comprehensive glutathione metabolism model,
29 facilitating the simulation of quinone redox cycling, and adduct-induced GSH depletion.
30 Simulations suggest that glutathione pools are most sensitive to exposure duration at
31 pharmacologically and supra-pharmacologically relevant doxorubicin concentrations. The
32 model provides an alternative method of investigating and quantifying redox cycling induced
33 oxidative stress, circumventing the experimental difficulties of measuring and tracking
34 radical species. This *in silico* framework provides a platform from which GSH depletion can
35 be explored as a function of a compound's physicochemical properties.

36

37 **Introduction**

38 Redox cycling describes the continuous reduction and oxidation cycle of a compound,
39 forming radical intermediates capable of transferring an electron to molecular oxygen,
40 generating the superoxide radical anion ($O_2^{\cdot-}$)¹. The dismutation of $O_2^{\cdot-}$ results in the
41 formation of hydrogen peroxide (H_2O_2), which can lead to elevated levels of other potentially
42 harmful reactive oxygen and nitrogen species (ROS, RNS)². Quinone species are arguably
43 the most renowned redox cyclers and are pivotal to many biological mechanisms³. For
44 example, quinone-based redox cycling facilitates electron transport within the mitochondria
45 via ubiquinone (Coenzyme Q), and is therefore essential to cellular bioenergetics⁴. However,
46 futile quinone redox cycling can lead to a cascade of ROS formation and as such, the link
47 between toxicity and quinone redox cycling is widely acknowledged⁵. Nevertheless, redox
48 cycling remains an understated mechanism of toxicity due to the fleeting existence of free
49 radical intermediates which hinders their quantification in real time, both *in vitro* and *in vivo*
50 ⁶. Potential redox cycling-based toxicity has been implicated with many compounds⁷. One

51 such quinone containing compound, doxorubicin, is an anthracycline drug used to treat a
52 variety of human cancers and is regarded as one of the most important chemotherapeutic
53 agents ⁸. However, the therapeutic utility of doxorubicin is undermined by its dose-dependent
54 cardiotoxicity, possibly arising as a result of futile redox cycling, with NADH dehydrogenase
55 within the mitochondria proposed as the most likely site of anthracycline reduction ^{9,10}.
56 Cellular glutathione plays a major role in the defence against redox cycling-derived oxidative
57 stress, either by direct interaction with ROS, RNS and electrophiles, or by acting as a co-
58 factor for various enzymes ^{11,12}. As a result, glutathione is at the forefront of mitigating
59 quinone-derived toxicity, by enzymatically reducing redox-generated H₂O₂ to harmless H₂O
60 via glutathione peroxidase, or by direct reaction and detoxification of the quinone
61 electrophile (Figure 1) ¹³⁻¹⁵.

62

63 The ability of a quinone to redox cycle is dependent upon the favourability of its reduction by
64 a single electron, which can be quantitatively described by its reduction potential (E^o). E^o is
65 the standard reduction potential in volts (V), when measured under standard conditions:
66 25°C, 1.0 M, pH 0.0 when in aqueous solution and at a pressure of 100 kPa (0.986 atm) ¹⁶.
67 The reduction potential can be described at non-standard conditions (i.e. physiological
68 conditions) using the Nernst Equation (Eq. 1), where E is the reduction potential at non-
69 standard conditions, $E^{o'}$ is the standard reduction potential at pH 7.0, R is the universal gas
70 constant (8.3145 J mol⁻¹ K⁻¹), T is the temperature of interest in Kelvin, F is the Faraday
71 constant (9.6485×10⁴ C mol⁻¹), n is the number of electrons in the reduction reaction and Q_r is
72 the reaction quotient for the half-cell reaction; equal to the ratio of the reduced and oxidised
73 species:

$$E = E^{o'} - \frac{R T}{n F} \ln Q_r . \quad (1)$$

74 The susceptibility of molecular oxygen to be reduced to O_2^- may also be described by its
75 reduction potential, shown in Equation (2). Specifically, the ability of a semiquinone radical
76 anion (SQ^-) to reduce molecular oxygen into superoxide can be quantified by linking both
77 reduction potentials ¹⁶.



78 The thermodynamic favourability of the reaction between SQ^- and molecular oxygen can
79 therefore be assessed by considering $E^{o'}$ for the (Q/ SQ^-) and (O_2 / O_2^-), where $E^{o'}$ (O_2 / O_2^-)
80 is -180 mV ¹⁷. The reaction equilibrium constant K_{eq} can also be calculated using Equation
81 (3):

$$E^{o'} \left(\frac{O_2}{O_2^-} \right) - E^{o'} \left(\frac{Q}{SQ^-} \right) = \frac{RT}{F} \ln K_{eq} \quad (3)$$

82 According to Equation (3), if $E^{o'}$ (Q/ SQ^-) is less than $E^{o'}$ (O_2 / O_2^-), then the equilibrium will
83 favour O_2^- formation (Equation (2)). Similarly, if $E^{o'}$ (Q/ SQ^-) is greater than $E^{o'}$ (O_2 / O_2^-)
84 then the opposite is true, favouring the reverse reaction, thereby leaving superoxide formation
85 thermodynamically unfavourable. However, it is important to recognise that these reactions
86 are reversible and therefore superoxide formation can occur even if the reverse rate is greater
87 than the forward rate. Within the cell, the production of superoxide is then a function of other
88 biological factors that influence the position of the equilibrium, such as, for example,
89 detoxification by superoxide dismutase enzymes (SOD) ^{3,18}.

90 The reductive addition reaction between Q and GSH is also linked to reduction potential
91 ($E^{o'}$), whereby the second order rate constant, dependent on the concentration of the
92 electrophile and GSH, ($\log(k/M^{-1} s^{-1})$) for the Michael reaction may be estimated ³. This is
93 extremely useful, as it provides a kinetic handle on the non-redox cycling quinone-derived
94 GSH depletion. Ultimately, toxicity is likely to present when the cellular antioxidant defense
95 mechanisms, such as glutathione metabolism, are overwhelmed. Indeed, depletion of cellular

96 GSH by 20 – 30% of normal has been shown to result in impaired oxidative stress defence
97 and lead to cell death¹⁹.
98 In this study, an *in silico* model of quinone metabolism was used to investigate how redox
99 cycling-induced ROS production and reductive addition GSH adduct formation impacts
100 glutathione homeostasis. This work aims to determine the significance of both quinone-based
101 GSH depletion mechanisms, as well as proposing a mathematical framework that can help
102 circumvent the experimental difficulty of quantifying reactive radical intermediates in real
103 time. Using doxorubicin as a training compound, three models of quinone redox cycling were
104 constructed, each capturing different potential redox cycling mechanisms. Each model was
105 fitted to oxygen consumption rate data, indicative of ROS formation, allowing the estimation
106 of unknown kinetic parameters, with the best fit model selected using variance-based
107 sensitivity analysis, the Akaike Information Criterion (AIC) and Bayesian Information
108 Criterion (BIC). The selected model was then expanded to include GS-H₂Q adduct formation,
109 estimating the required kinetic formation parameter from its reduction potential, $E^{o'}$, before
110 being combined with a previously published model of glutathione metabolism. The combined
111 model was used to simulate the subsequent GSH depletion as a function ROS generated from
112 redox cycling and adduct formation for a single and extended exposure of doxorubicin.

113

114 **Materials and Methods**

115 ***In silico***

116 **Model construction**

117 Three *in silico* quinone redox metabolism models were proposed, each representing different
118 potential redox cycling mechanisms (Figure 2). The first model, hereafter referred to as the
119 reduced model, is a reduced representation describing the cycling between the parent quinone

120 (Q) and semiquinone radical anion (SQ⁻), as well as superoxide (O₂⁻) and hydrogen peroxide
121 (H₂O₂) formation. The second model (triad model) represents the classical triad of quinone
122 redox cycling, expanding the reduced model to include the transformation between the
123 semiquinone radical anion and fully reduced hydroquinone. The third model
124 (comproportionation model) expands the triad model to include the comproportionation
125 reaction, whereby two semiquinone radicals can reform the parent quinone compound and
126 hydroquinone species. A schematic of each model is shown in Figure 2, with the
127 corresponding kinetic rate equations described in Table 1.

128

129 **Model kinetic terms, parameters and initial conditions**

130 Quinone redox reaction kinetics were described according to the law of mass action such that
131 the rate of reaction is proportional to the concentration of the reactants for a given a rate
132 constant, with k_{pn} and k_{mn} representing the forward rate and reverse rate constants respectively
133 and n denotes the considered reaction (1-5; Table 1). Initial-conditions, fitted parameter
134 values and ordinary differential equations (ODEs) are provided in the supplementary
135 information. The model ODEs were solved in MATLAB[®] 2017a via numerical integration
136 using the variable-order stiff solver ode15s.

137

138 **Model selection: AIC-BIC criteria**

139 Model selection was directed using the Akaike Information Criterion (AIC) and Bayesian
140 Information Criterion (BIC). AIC and BIC values examine how fitted model solutions
141 compare to the experimental OCR data. Both AIC and BIC values are penalised-likelihood
142 criterion that consider model complexity (e.g. number of parameter values) and are
143 commonly used during model selection²⁰. For example, AIC and BIC values may suggest

144 that a less complex model (fewer parameters) may be the most appropriate model to use, even
145 if a more complex model fits the data better.

146 **GSH metabolism expansion**

147 Expansion of the selected model to include adduct formation (Equation (4)) was achieved by
148 estimating the reaction rate constant, k_{QGS} , from Figure 12 in the work by Song. et al. ³,
149 using the doxorubicin-specific $E^{o'}$ (-292 to -341 mV). This particular figure demonstrates
150 how the rate constants for the Michael addition of glutathione with various quinones are a
151 function of the $E^{o'}$ with a linear relationship.



152 Simulating the effects of redox cycling and adduct formation on GSH homeostasis was
153 achieved by extending the triad quinone metabolism model to include a complete
154 representation of glutathione metabolism. A full curated version of the GSH metabolism
155 model developed by Reed et al. ²¹ was downloaded from the BioModels Database and
156 amended for simulation and coupling to the quinone metabolism model in MATLAB.
157 Specifically, the Reed model and quinone redox cycling models were coupled via the H_2O_2 ,
158 Q and GSH variables. Model H_2O_2 is generated from quinone redox cycling / hydroquinone
159 auto-oxidation, being detoxified by glutathione peroxidase, and Q and GSH removal is a
160 function of adduct formation (Michael reaction). The amended ODEs for H_2O_2 , GSH and Q
161 are as follows:

162

163

164

165

166

167

$$\frac{d[H_2O_2]}{dt} = R_3 - V_{GPx} + R_6,$$

$$\frac{d[GSH]}{dt} = V_{GS} - V_{cgshHb} - V_{cgshLb} - 2 V_{GPx} + 2 V_{GR} - V_{gshdeg} - R_5,$$

$$\frac{d[Q]}{dt} = -R_1 + R_2 - R_5,$$

168 where, $R_5 = [Q][GSH]k_{QGSH}$ and $R_6 = [O_2^-]^2k_{SOD}$.

169 The rate equations for V_{GS} , V_{cgshHb} , V_{cgshLb} , V_{GPx} , V_{GR} and V_{gshdeg} are taken from Reed et al.
170 ²¹ and located within the supplementary information, along with the full details of their
171 model. The successful combination of this model with the redox cycling model was proven
172 by recapitulation of Figures 2 and 6 from the Reed et al. publication ²¹, shown in the
173 supplementary information.

174 **Quinone redox metabolism model assumptions**

175 Like all mathematical models, this biochemical redox cycling model is based upon a set of
176 assumptions regarding biological and chemical space. The model assumes that the electrons
177 and factors mediating reductive processes, such as reductase enzymes, are abundant and that
178 doxorubicin reduction occurs readily. Furthermore, the concomitant rate of auto-oxidation of
179 doxorubicin within the cell is assumed to be equal to that of the OCR experimental data used
180 to parameterise the model.

181 **Experimental**

182 **Materials**

183 All extracellular flux analysis consumables were purchased from Agilent (North Billerica,
184 MA, USA). Doxorubicin was purchased from Sigma Aldrich (Dorset, UK).

185 **Extracellular flux analysis (EFA)**

186 The utility plate was calibrated according to manufacturer instructions on the day before the
187 assay. Doxorubicin stock solution (10 mM, 100 % DMSO) was serially diluted in unbuffered

188 seahorse assay medium to prepare 6 concentrations: 400, 300, 200, 100, 80 and 40 μM .
189 Compound solutions were set to a final pH of 7.0 using HCl and KOH when necessary. Final
190 compound dilution occurs post-injection giving a final concentration of 50, 35, 25, 12.5, 10
191 and 5 μM inside the well.
192 On the day of the assay, doxorubicin working solutions were added to injection port A of
193 each well of the sensor cartridge (25 μL). The instrument was then calibrated according to the
194 manufacturer's instructions. Prior to analysis, the XFe96 instrument (Seahorse Biosciences,
195 North Billerica, MA, USA) mixed the assay media in each well for 10 minutes to allow the
196 oxygen partial pressure to reach equilibrium. Extracellular flux analysis was conducted
197 simultaneously measuring the extracellular acidification rate ECAR via proton production
198 rate (PPR) and oxygen consumption rate (OCR). The first three measurements were used to
199 establish a baseline rate. All measurements include a 3-minute mix, allowing the probe to
200 retract and collapse the transient micro chamber. This allows oxygen tension and pH in the
201 microenvironment to restore to normal. Doxorubicin was injected after the third measurement
202 (16 minutes) and the resulting changes in PPR and OCR were measured for a further 20
203 measurements (over 150 minutes) yielding the basal response.

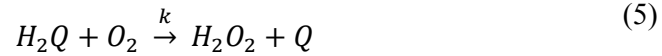
204 **Results**

205 **Experimental**

206 **Extracellular flux analysis: oxygen consumption rate (OCR)**

207 Extracellular flux analysis was used to measure the oxygen consumption rate before and after
208 injection of doxorubicin into unbuffered XF media at pH 7.0 (Figure 3). Doxorubicin (50,
209 37.5, 25, 12.5 and 10 μM) was injected into the media 16 minutes into the experiment
210 (between measurements 1 and 2), yielding concentration-dependent oxygen consumption
211 profiles in a cell-free environment. Oxygen consumption has long been attributed to
212 hydroquinone auto-oxidation and the formation of H_2O_2 and $\text{O}_2^{\cdot-}$ ^{3,5,22}. Auto-oxidation refers

213 to oxidation in the absence of a metal catalyst and in this instance, the oxygen consumption
214 rate data represents doxorubicin hydroquinone (Figure 1b) auto-oxidation²³. Hydroquinone
215 auto-oxidation yields stoichiometric production of H₂O₂, shown in Equation (5).



216

217 Note, Equation (5) is not intended to describe the complete oxidation mechanisms by which
218 hydroquinone auto-oxidates to generate H₂O₂. The actual mechanism is likely to occur via
219 two sequential steps with semiquinone (SQ⁻) and superoxide (O₂⁻) intermediates. Rather, it
220 aims to provide concise stoichiometric representation of the formation of H₂O₂ from H₂Q
221 auto-oxidation.

222 ***In silico***

223 **Model fitting and selection: AIC BIC Criterion**

224 The oxygen consumption rate (OCR) data generated in Figure 3 provides an experimental
225 platform for the parameterisation of the mathematical models. The OCR data indirectly
226 corresponds to H₂O₂ production, via the superoxide formation reaction shown in Equation
227 (6). Within the models, the dynamics of O₂ are not explicitly specified but rather, assumed to
228 be constant as k_{O_2} , due to a separation of scales. Consequently, OCR is then represented by
229 the R_2 reaction flux, as shown in Equation (6).

$$OCR = R_2 = k_{p2} [SQ^-]k_{O_2} - k_{m2} [Q] [O_2^-]. \quad (6)$$

230 The reduced, triad and comproportionation models were fit to the 37.5 and 25 μM (training
231 concentrations) OCR data profiles from Figure 3 via the R_2 reaction flux shown in Equation
232 (6). The 50, 12.5 and 10 μM data (test concentrations) were withheld to be used for blind
233 validation. The unknown rate constants for R_1 , R_2 , R_3 , R_4 and R_5 for the respective models
234 were fitted using the LSQNONLIN function in MATLAB, a non-linear least squares solver.

235 The performance of each model was compared by examining how close the predicted
236 solutions were to the experimental OCR data using the penalised-likelihood AIC and BIC
237 criteria. AIC and BIC values are representative of the distance between the fitted likelihood
238 of the model and the unknown true likelihood function of the data, with the BIC criterion
239 penalising model complexity more heavily than the AIC^{20,24}. Table 2 shows the computed
240 AIC and BIC values, illustrating that the reduced model returns a much higher score than the
241 triad and comproportionation models. However, the AIC and BIC values for the triad and
242 comproportionation models are very similar. Therefore, this criterion was deemed conclusive
243 enough to discount the reduced model as a viable model for describing the OCR data, but
244 insufficient to prompt selection of either the triad or comproportionation model.

245

246 **Sensitivity analysis: Model selection**

247 Global sensitivity analysis (GSA) was conducted using the classical Sobol method. This
248 variance-based method is concerned with the decomposition of the output variance and
249 attributing this variance to input factors^{25,26}. In this instance, GSA was performed to quantify
250 the influence of all model parameters on model OCR output (Figure 4), facilitating selection
251 of either the triad or comproportionation model.

252

253 The results of the global sensitivity analysis for the redox cycling parameters with respect to
254 model OCR output are shown in Figure 4. Normal distributions were applied to all inputs,
255 with the mean obtained from the previous optimisation procedure, and coefficient of variation
256 of 180%. First order main effect indices and the total-order indices were computed. The main
257 effect indices are equivalent to direct variance-based measures; they measure the effect of
258 varying an input factor alone, averaged over variations in all other inputs. The total effect
259 indices provide the contribution of variance in a parameter including the variance of all

260 possible higher order interactions, indicating the importance of any input. The use of total
261 effect indices negates the need for determining higher order interactions which can be
262 computationally expensive. The sensitivity of the forward rate constants for the superoxide
263 formation reaction, k_{p2} , and the oxygen concentration parameter, k_{O2} , proved to be the most
264 sensitive globally with respect to total effects, highlighted in Figure 4. Furthermore, both k_{p2}
265 and k_{O2} register as the two most sensitive parameters with respect to the main effects, with k_{p4}
266 also sensitive. The sensitivity of R_4 parameters (k_{p4}) with respect to model OCR output is in
267 good accordance with the AIC/BIC analysis, confirming the need for the R_4 reaction, which is
268 present in both the triad and the comproportionation models, but not in the reduced model.
269 This suggests that the reformation of the SQ^- from H_2Q is mechanistically important during
270 the redox metabolism of doxorubicin.

271 The global sensitivity analysis suggests that the comproportionation reaction, R_5 , is not
272 pivotal for the model OCR output, given that its parameters, k_{p5} and k_{m5} , are the two least
273 sensitive parameters for both main and total interactions. This finding prompted the selection
274 of the triad model, given that first; R_4 is required to adequately model OCR output, illustrated
275 in both the AIC/BIC analysis and GSA, second; that model OCR output is insensitive to the
276 inclusion of the comproportionation kinetics (R_5) and finally; the triad model is simpler,
277 requiring estimation of fewer parameters.

278 **Triad model validation**

279 Figure 5 compares the simulated triad model OCR output with the experimental OCR data.
280 The model was first fitted to the “training concentrations” (37.5 and 25 μ M doxorubicin), and
281 then used to simulate the “test concentrations” (50, 12.5 and 10 μ M doxorubicin) as a means
282 of blind validation, showing good accordance between the experimental and *in silico* outputs
283 for all concentrations of doxorubicin. The simulated profiles for the reduced and

284 comproportionation models, as well as the parameter values generated from the fitting
285 process, are located in the supplementary information.

286 **Combined triad-GSH metabolism model simulations: quinone metabolism and ROS**
287 **production**

288 Following the parameterisation and sensitivity analysis, the triad model was expanded to
289 include GS-H₂Q adduct formation (quinone removal) and was combined with the glutathione
290 metabolism model constructed by Reed et al.²¹. The combined model output was validated
291 by replicating Figures 2 and 6 from the Reed et al. publication (shown in the supplementary
292 information) in order to confirm that; i), the model obtained from the BioModels Database
293 can recapitulate the figures that were not used for its curation, and ii) that addition of the triad
294 model does not affect the glutathione metabolism model output when no doxorubicin is
295 present.

296 A major benefit of implementing an *in silico* approach to investigating quinone metabolism is
297 the ability to simulate and visualise radical species, such as superoxide, in real time, as this is
298 essentially inaccessible experimentally both *in vitro* and *in vivo*. Figure 6 presents the
299 simulated fate of a single 50 µM doxorubicin exposure (top panel), as well as the subsequent
300 O₂⁻ and H₂O₂ profiles, over a 30-minute time-span. The model predicts that a single 50 µM
301 exposure will yield a rapid but small increase in H₂Q and SQ⁻ of 5.57 µM and 2.10 µM
302 respectively, with all three forms of the quinone requiring 30 minutes to be removed by GSH
303 from the system.

304
305 **Combined triad-GSH metabolism model simulations: impact of quinone metabolism on**
306 **glutathione homeostasis**

307 The model was used to investigate how single *vs* constant 50 µM exposure of doxorubicin
308 influenced blood and cytosolic GSH and cysteine (Cys) levels, over a 10-hour time-span,
309 shown in Figure 7. A single exposure (A) causes a small decrease (less than 3% of normal),

310 in both blood and cytosolic GSH and Cys concentrations, with levels returning to above 99%
311 of normal for all species within the simulated time-span. Cytosolic Cys experiences the
312 greatest decrease after a single exposure, which is indicative of the model facilitating rapid
313 GSH re-synthesis after an initial depletion. While cytosolic and blood GSH and Cys
314 biochemical species all experience depletion, the model predicts that a single exposure to
315 doxorubicin only results in a minimal perturbation of the antioxidant defence system. In
316 contrast, a constant 50 μM exposure of quinone (B) overwhelms blood and cytosolic GSH
317 and Cys, showing no signs of recovery after a 10-hour time-span. Specifically, simulations
318 suggest that blood Cys and GSH are reduced by 68.7% and 74.1% respectively, whereas
319 cytosolic Cys and GSH are reduced by 81.2% and 64.6% respectively. While a constant
320 exposure of quinone is not necessarily representative of an *in vivo* scenario, it is however,
321 much more representative of an *in vitro* situation, whereby a constant source of quinone is
322 essentially available in the extracellular media during cell culture²⁷. Therefore, the model
323 provides a platform from which the impact of varying degrees of quinone concentration and
324 exposure times on GSH homeostasis may be computationally examined.

325 A practical application of the combined model would be to predict the concentration and
326 exposure time required to cause toxicity via overwhelming GSH metabolism as a function of
327 quinone metabolism. As such, the model was used to simulate how long it would take
328 pharmacologically and toxicologically relevant concentrations of doxorubicin to yield a 70%
329 reduction in GSH concentration, indicative of impaired cellular antioxidant defence, protein
330 binding and cell death¹⁹.

331 Figure 8 illustrates how a single exposure vs constant infusion of a wide range of doxorubicin
332 concentrations (0-50 μM) affects cytosolic GSH concentration. The simulation time-span was
333 extended to 20 hours in order to discern what exposure time and concentration would yield a
334 70% of normal reduction of GSH. A single exposure of doxorubicin between 0 and 50 μM ,

335 yields minimal cytosolic GSH depletion (2.5% maximum decrease), which recovers within
336 the prescribed time-span (Figure 8A). However, for the same concentration range, a constant
337 exposure can yield a harmful depletion of GSH to 30% of normal after 14 hours, indicated by
338 the black-dashed line (Figure 8B).

339

340 **Discussion**

341 A mathematical modelling approach was deployed to simulate GSH depletion as a function
342 of doxorubicin redox metabolism. The predominant motivation for mathematically modelling
343 quinone redox metabolism was to facilitate the investigation of experimentally difficult
344 scenarios; specifically, the fleeting existence of radical species and the rapid rate at which
345 redox cycling can generate ROS, causing oxidative stress^{5,7,28}. Doxorubicin was selected as a
346 training compound for three reasons: i) the quinone moiety, present in doxorubicin, is
347 acknowledged as a notorious redox cyler; ii) doxorubicin also contains the hydroquinone
348 moiety as part of its chemical structure, allowing auto-oxidation to be used as a
349 parameterisation method for a potential redox cycle; and iii) doxorubicin itself has long been
350 implicated with futile redox cycling toxicity, specifically within the mitochondria²⁹.
351 Mathematically modelling redox cycling is difficult because of the different potential
352 mechanisms through which the process may occur. However, these difficulties were reduced
353 by first considering three models (Figure 2), with increasing degrees of mechanistic
354 complexity, to be aligned with the experimental data. This method allowed the goodness of
355 fit to inform upon an appropriate model structure when the actual reaction rates were
356 unknown and, in doing so, provided a useful indication of the possible mechanism by which
357 this process occurs. Appropriate model assumptions facilitated initial model reduction by
358 capturing only the essential elements of the system. In this study, it was assumed that using
359 the auto-reduction of the hydroquinone adjacent to the quinone on doxorubicin was a

360 sufficient indicator of the rate of oxidation of a potential redox cycle, either on the
361 hydroquinone or the quinone after reduction. Indeed, experimental analysis showed that
362 introduction of doxorubicin into physiologically relevant pH media yielded a concentration-
363 dependent oxygen consumption profile, revealing free (non-metal catalysed) auto-oxidation
364 (Figure 3). This finding was in good accordance with the literature, where the hydroquinone
365 is routinely shown to auto-oxidate under these conditions^{30,31}.

366 AIC and BIC model selection criteria were deployed to suggest which model is
367 mechanistically important, guided by the OCR data. The analysis revealed that both the
368 comproportionation and triad models were better suited to represent the experimental data
369 than the reduced model, but were inconclusive with respect to overall model selection, given
370 that both AIC/BIC values were extremely similar (Figure 4). The triad model was selected as
371 the final model as the comproportionation reaction (R_5) parameters (k_{p5} and k_{m5}) were the two
372 least sensitive parameters with respect to model OCR output for both main and total effects
373 during global sensitivity analysis (Figure 4). While the comproportionation reaction is a well
374 reported redox cycling chemical mechanism, in this instance the triad model does not require
375 the additional comproportionation reaction to accurately replicate the experimental OCR
376 profile, suggesting that the comproportionation reaction is not mechanistically integral to the
377 production of ROS through a quinone-based redox cycle. Omission of the
378 comproportionation kinetics by selecting the triad model also reduces the number of
379 parameters that require estimating, reducing uncertainty in the overall parameter space.

380 Global sensitivity analysis revealed that k_{O_2} (oxygen concentration) is the most sensitive
381 parameter for OCR and ROS output, suggesting that biological environments with elevated
382 oxygen presence could be more susceptible to redox-induced ROS. Indeed, the association of
383 doxorubicin with bioenergetic toxicity is well stated in the literature³²⁻³⁴. The global
384 sensitivity analysis also confirmed the importance of the redox cycle between SQ^- and H_2Q

385 (R_4), showing that the reverse rate constant, k_{m4} (SQ^- reformation), was the second most
386 sensitive (main interactions) with respect to model OCR and therefore ROS production,
387 suggesting auto-oxidation is an essential part of the doxorubicin redox mechanism. The triad
388 model captures the OCR data for all concentrations of doxorubicin, simulating auto-oxidation
389 via the formation of SQ^- and O_2^- intermediates, which is in good accordance with the
390 literature³. While the simulations are confined by these assumptions, it is worth noting that
391 redox cycling is governed by thermodynamics, which according to the reduction potential of
392 doxorubicin, are favourable with respect to the formation of superoxide should a semiquinone
393 radical species be present³.

394 After the model was expanded to include GS- H_2Q adduct formation as a function of its
395 reduction potential, it was then combined with the Reed glutathione model²¹ in order to
396 simulate how the quinone redox-metabolism of doxorubicin influenced the glutathione
397 metabolism. The combined model presented here effectively extends the work of Reed et al.
398 to investigate how quinone redox metabolism can cause toxicity through GSH depletion. The
399 Reed model provides a comprehensive mathematical representation of one-carbon GSH
400 metabolism, boasting the inclusion of the transsulfuration pathway, as well as glutathione
401 synthesis, transport and breakdown. Model curation provides researchers with the ability to
402 obtain, adapt and implement such mathematical models, as outlined in this study, and is
403 therefore a powerful tool in the arsenal of any systems biologist, pharmacologist or
404 toxicologist. The combined model first provided visualisation of quinone redox-metabolism
405 by capturing the transitions between Q, SQ^- and H_2Q , as well as the subsequent production of
406 O_2^- over a 30-minute time-span. Note that semiquinone radicals can possess extremely long
407 half-lives, up to days at 37°C³⁵, and as such, it is unsurprising that SQ^- is present over 30
408 minutes in the model (Figure 6). The simulations suggested that quinone metabolism yielded
409 an increase in ROS (O_2^- and H_2O_2), producing a maximum of 0.42 μM and 1×10^{-3} μM

410 respectively. Interestingly, despite the presence of superoxide dismutase (SOD) ($k = 2.4 \times 10^9$
411 $\text{M}^{-1} \text{s}^{-1}$)³⁶, the resulting concentration of H_2O_2 is significantly smaller than the concentration
412 of superoxide, indicating that the model is able to respond well to a transient increase in ROS,
413 maintaining low H_2O_2 concentrations. It is important to note that current *in vitro* redox
414 cycling detection is centred on indirect quantification of H_2O_2 production and O_2
415 consumption rather than direct measurement of dynamic radical species over time^{22,28}.

416 The model predicted that for 10-hour-long toxicologically relevant doxorubicin ($50 \mu\text{M}$)
417 simulations, the duration of the exposure is more important than concentration with respect to
418 overwhelming glutathione metabolism. The consideration of cysteine during these
419 simulations were important, as cytosolic cysteine is the rate limiting amino acid precursor for
420 synthesis of GSH, via the γ -glutamylcysteine synthetase (GCS) enzyme, and this is a function
421 of its reduced concentration compared to the other precursors, glycine and glutamate.

422 Consequently, cysteine availability and the resulting GCS activity are both pivotal for GSH
423 re-synthesis and therefore provide an indication of the model's potential to recover GSH
424 levels²¹.

425 Further simulations showed that over a wide range of doxorubicin (0 - $50 \mu\text{M}$), the model can
426 be used to suggest the specific concentration and exposure duration required to deplete
427 cytosolic GSH by 70%, the threshold by which antioxidant defence is impaired, protein
428 binding occurs, and cell death is possible. A broad range was considered in order to explore
429 the supra-pharmacological ($>10 \mu\text{M}$) concentrations required to induce toxicity, as well as the
430 effects of more pharmacologically relevant values (0.1 - $1.0 \mu\text{M}$) for an extended duration¹⁰.

431 The influence doxorubicin has on GSH depletion is most certainly also dependent upon the
432 cell-type and tissue-type in question. For example, lung cancer cell-lines show different
433 sensitivities to doxorubicin in the form of GSH depletion, with A549 and GLC₄210(S) cells
434 experiencing approximately 50% and 64% GSH depletion after a 12 hour exposure to 70 nM

435 and 5 nM (per million cells) respectively ³⁷. However, HeLa cells are much more sensitive,
436 with 2.5 nM (per million cells) of doxorubicin resulting in up to 80% GSH depletion for the
437 same exposure time ³⁸. Some cell-types are much less sensitive to doxorubicin-induced GSH
438 depletion. Hepatocytes treated with 111 μ M for 4 hours experience an approximate 20%
439 decrease in both cytoplasmic and mitochondrial GSH ³⁹. Our model simulations are reflective
440 of the hepatic GSH environment, agreeing with the supra-pharmacological concentrations of
441 doxorubicin required to illicit comparable GSH depletion in the liver ³⁹. Indeed, the original
442 GSH metabolism constructed by Reed et al. explores the properties of glutathione
443 metabolism in the liver ²¹, therefore lending confidence to our predictions. Training a
444 mathematical model to other specific cell-lines is possible and beneficial to reveal phenotypic
445 heterogeneity in metabolic properties. Such methodology has been successfully applied ⁴⁰,
446 and could be implemented in this framework to investigate specific cell and tissue types.
447 The modelling approach we have utilised in this study facilitates the exploration of potential
448 toxicity based on a compound's physicochemical properties, in this instance the reduction
449 potential. The ability to predict compound concentrations and exposure durations that could
450 cause a significant compromise in cellular antioxidant defence as a function of a
451 physicochemical property, especially with respect to an understated mechanism such as redox
452 cycling, could prove to be extremely useful when investigating toxicity with the reduction of
453 animal models in mind. In this instance, the concentrations of doxorubicin required to induce
454 a deleterious GSH response fall firmly outside of the therapeutic ranges of circulating
455 doxorubicin reported ⁴⁰. Consequently, simulations suggest that while doxorubicin redox
456 metabolism impacts GSH metabolism, the concentrations required to illicit a toxic response,
457 with either a single or extended exposure, reside outside that of the therapeutic dosing range.
458 This finding agrees with the literature whereby the role of quinone redox metabolism is an
459 ambiguous source of toxicity, with evidence suggesting that redox cycling requires supra-

460 pharmacological concentrations of doxorubicin to generate substantial ROS in tissues and
461 cells¹⁰.
462 Overall, the combined model demonstrates the utility of high quality previously published
463 models when constructing a framework to investigate a specific toxicity. The combined
464 quinone redox – glutathione metabolism model can be used to simulate experimentally
465 challenging scenarios such as potential redox cycling toxicity, while providing a platform
466 from which quinone exposure and concentration toxicity experiments may be guided.
467 Furthermore, the construction of mathematical frameworks such as this can be implemented
468 to explore other classes of compounds and mechanisms of toxicity as a function of their
469 physicochemical properties, while providing an alternative method of quantifying
470 experimentally elusive radical species.

471

472 **Data availability**

473 All model parameters and kinetic information are presented in the supplementary
474 information. Experimental oxygen consumption rate data is provided as an additional file.

475

476 **References**

- 477 1. Dudka, J. *et al.* Intensification of Doxorubicin-Related Oxidative Stress in the Heart by
478 Hypothyroidism Is Not Related to the Expression of Cytochrome P450 NADPH-
479 Reductase and Inducible Nitric Oxide Synthase, As Well As Activity of Xanthine
480 Oxidase. *Oxid. Med. Cell. Longev.* **2012**, 139327 (2012).
- 481 2. Clement, M. V & Pervaiz, S. Intracellular superoxide and hydrogen peroxide
482 concentrations: a critical balance that determines survival or death. *Redox Rep.* **6**, 211–
483 214 (2001).

- 484 3. Song, Y. & Buettner, G. R. Thermodynamic and kinetic considerations for the reaction
485 of semiquinone radicals to form superoxide and hydrogen peroxide. *Free Radic. Biol.*
486 *Med.* **49**, 919–962 (2010).
- 487 4. Nohl, H. Is redox-cycling ubiquinone involved in mitochondrial oxygen activation?
488 *Free Radic. Res. Commun.* **8**, 307–315 (1990).
- 489 5. Cohen, G. M. & d’Arcy Doherty, M. Free radical mediated cell toxicity by redox
490 cycling chemicals. *Br. J. Cancer. Suppl.* **8**, 46–52 (1987).
- 491 6. Halliwell, B. & Whiteman, M. Measuring reactive species and oxidative damage in
492 vivo and in cell culture: how should you do it and what do the results mean? *Br. J.*
493 *Pharmacol.* **142**, 231–255 (2004).
- 494 7. Rana, P., Naven, R., Narayanan, A., Will, Y. & Jones, L. H. Chemical motifs that
495 redox cycle and their associated toxicity. *Medchemcomm* **4**, 1175–1180 (2013).
- 496 8. Zhang, S. *et al.* Identification of the molecular basis of doxorubicin-induced
497 cardiotoxicity. *Nat. Med.* **18**, 1639 (2012).
- 498 9. Davies, K. J. A. & Doroshov, J. H. Redox cycling of anthracyclines by cardiac
499 mitochondria. I. Anthracycline radical formation by NADH dehydrogenase. *J. Biol.*
500 *Chem.* **261**, 3060–3067 (1986).
- 501 10. Zhu, H. *et al.* Doxorubicin Redox Biology: Redox Cycling, Topoisomerase Inhibition,
502 and Oxidative Stress. *React. Oxyg. Species* 189–198 (2016).
503 doi:10.20455/ros.2016.835
- 504 11. Pastore, A., Federici, G., Bertini, E. & Piemonte, F. Analysis of glutathione:
505 implication in redox and detoxification. *Clin. Chim. Acta* **333**, 19–39 (2003).
- 506 12. Robaczewska, J. *et al.* Role of glutathione metabolism and glutathione-related
507 antioxidant defense systems in hypertension. *J. Physiol. Pharmacol.* **67**, 331–337
508 (2016).

- 509 13. Brunmark, A. & Cadenas, E. Reductive addition of glutathione to p-benzoquinone, 2-
510 hydroxy-p-benzoquinone, and p-benzoquinone epoxides. Effect of the hydroxy- and
511 glutathionyl substituents on p-benzohydroquinone autoxidation. *Chem. Biol. Interact.*
512 **68**, 273–298 (1988).
- 513 14. Lau, S. S., Hill, B. A., Highet, R. J. & Monks, T. J. Sequential oxidation and
514 glutathione addition to 1,4-benzoquinone: Correlation of toxicity with increased
515 glutathione substitution. *Mol. Pharmacol.* **34**, 829–836 (1988).
- 516 15. Monks, T. J. & Lau, S. S. Toxicology of Quinone-Thioethers. *Crit. Rev. Toxicol.* **22**,
517 243–270 (1992).
- 518 16. Wardman, P. Reduction Potentials of One-Electron Couples Involving Free Radicals
519 in Aqueous Solution. *J. Phys. Chem. Ref. Data* **18**, 1637–1755 (1989).
- 520 17. Koppenol, W. H., Stanbury, D. M. & Bounds, P. L. Electrode potentials of partially
521 reduced oxygen species, from dioxygen to water. *Free Radic. Biol. Med.* **49**, 317–322
522 (2010).
- 523 18. Song, Y. *et al.* Chlorination increases the persistence of semiquinone free radicals
524 derived from polychlorinated biphenyl hydroquinones and quinones. *J. Org. Chem.*
525 **73**, 8296–8304 (2008).
- 526 19. Rang, H. P., Ritter, J. M., Flower, R. J., Henderson, G. AND Dale, M. M. *Rang and*
527 *Dale's Pharmacology*. (Elsevier, 2016).
- 528 20. Chakrabarti, A. & Ghosh, J. K. AIC, BIC and Recent Advances in Model Selection. in
529 *Handbook of the Philosophy of Science* (eds. Bandyopadhyay, P. S. & Forster, M. R.
530 B. T.-P. of S.) **7**, 583–605 (North-Holland, 2011).
- 531 21. Reed, M. C. *et al.* A mathematical model of glutathione metabolism. *Theor. Biol. Med.*
532 *Model.* **5**, 8 (2008).
- 533 22. Winston, G. W., Church, D. F., Cueto, R. & Pryor, W. A. Oxygen Consumption and

- 534 Oxyradical Production from Microsomal Reduction of Aqueous Extracts of Cigarette
535 Tar. *Arch. Biochem. Biophys.* **304**, 371–378 (1993).
- 536 23. Miller, D. M., Buettner, G. R. & Aust, S. D. Transition metals as catalysts of
537 “autoxidation” reactions. *Free Radic. Biol. Med.* **8**, 95–108 (1990).
- 538 24. Wei, J. & Zhou, L. Model selection using modified AIC and BIC in joint modeling of
539 paired functional data. *Stat. Probab. Lett.* **80**, 1918–1924 (2010).
- 540 25. Patelli, E. COSSAN: A Multidisciplinary Software Suite for Uncertainty
541 Quantification and Risk Management. in *Handbook of Uncertainty Quantification*
542 (eds. Ghanem, R., Higdon, D. & Owhadi, H.) 1–69 (Springer International Publishing,
543 2016). doi:10.1007/978-3-319-11259-6_59-1
- 544 26. Patelli, E., Pradlwarter, H. J. & Schuëller, G. I. Global sensitivity of structural
545 variability by random sampling. *Comput. Phys. Commun.* **181**, 2072–2081 (2010).
- 546 27. Falgreen, S. *et al.* Exposure time independent summary statistics for assessment of
547 drug dependent cell line growth inhibition. *BMC Bioinformatics* **15**, 168 (2014).
- 548 28. Adam, A., Smith, L. L. & Cohen, G. M. An assessment of the role of redox cycling in
549 mediating the toxicity of paraquat and nitrofurantoin. *Environ. Health Perspect.* **85**,
550 113–117 (1990).
- 551 29. Malhi, S. S. *et al.* Intracellular delivery of redox cyler-doxorubicin to the
552 mitochondria of cancer cell by folate receptor targeted mitocancerotropic liposomes.
553 *Int. J. Pharm.* **432**, 63–74 (2012).
- 554 30. Roginsky, V. & Barsukova, T. Kinetics of oxidation of hydroquinones by molecular
555 oxygen. Effect of superoxide dismutase. *J. Chem. Soc. Perkin Trans. 2* 1575–1582
556 (2000). doi:10.1039/B000538J
- 557 31. LuVALLE, J. E. & WEISSBERGER, A. Oxidation processes; quinone catalysis in the
558 autoxidation of hydroquinones. *J. Am. Chem. Soc.* **69**, 1576–1582 (1947).

- 559 32. Gorini, S. *et al.* Chemotherapeutic Drugs and Mitochondrial Dysfunction: Focus on
560 Doxorubicin, Trastuzumab, and Sunitinib. *Oxid. Med. Cell. Longev.* **2018**, 7582730
561 (2018).
- 562 33. Ichikawa, Y. *et al.* Cardiotoxicity of doxorubicin is mediated through mitochondrial
563 iron accumulation. *J. Clin. Invest.* **124**, 617–630 (2014).
- 564 34. Pereira, G. C. *et al.* Drug-induced cardiac mitochondrial toxicity and protection: From
565 doxorubicin to carvedilol. *Curr. Pharm. Des.* **17**, 2113–2129 (2011).
- 566 35. Kehrer, J. P., Robertson, J. D. & Smith, C. V. 1.14 - Free Radicals and Reactive
567 Oxygen Species. in (ed. McQueen, C. A. B. T.-C. T. (Second E.) 277–307 (Elsevier,
568 2010). doi:<https://doi.org/10.1016/B978-0-08-046884-6.00114-7>
- 569 36. Winterbourne, C.C , French, J.K, Claridge, R. F. . Superoxide Dismutase as an
570 Inhibitor of Reactions of Semiquinone Radicals. *FEBS Lett.* **94**, (1978).
- 571 37. al-Kabban, M., Stewart, M. J., Watson, I. D. & Reglinski, J. The effect of doxorubicin
572 on the glutathione content and viability of cultured human lung cancer cell lines A549
573 and GLC4 210. *Clin. Chim. Acta.* **194**, 121–129 (1990).
- 574 38. al-Kabban, M. *et al.* The use of 1H spin echo NMR and HPLC to confirm doxorubicin
575 induced depletion of glutathione in the intact HeLa cell. *Br. J. Cancer* **57**, 553–558
576 (1988).
- 577 39. Meredith, M. J. & Reed, D. J. Depletion in vitro of mitochondrial glutathione in rat
578 hepatocytes and enhancement of lipid peroxidation by adriamycin and 1,3-bis(2-
579 chloroethyl)-1-nitrosourea (BCNU). *Biochem. Pharmacol.* **32**, 1383–1388 (1983).
- 580 40. McKenna, M. T. *et al.* A Predictive Mathematical Modeling Approach for the Study of
581 Doxorubicin Treatment in Triple Negative Breast Cancer. *Sci. Rep.* **7**, 5725 (2017).
582
583

584 **Acknowledgements**

585 R.A.K. acknowledges funding support from a BBSRC Industry Case Partnership with GSK
586 (BB/L502273/2), <https://bbsrc.ukri.org>, <https://www.gsk.com>. J.L. and S.D.W acknowledge
587 funding support from the EPSRC Liverpool Centre for Mathematics in Healthcare
588 (EP/N014499/1), <https://epsrc.ukri.org>. The funders had no role in study design, data
589 collection and analysis, decision to publish, or preparation of the manuscript. We thank Dr
590 Carol Jolly (University of Liverpool) for advice and set-up of the extracellular flux analysis
591 assay.

592 **Author contributions**

593 S.W and R.K contributed to the conception and design of the study and final approval of the
594 version to be submitted. R.K, J.L and S.W conducted the mathematical modelling aspects of
595 the study, with D.C and R.K performing the sensitivity analysis using the COSSAN suite.
596 Experimental work was conducted by R.K and designed by R.K and A.C. S.E provided
597 chemistry guidance. A.H provided industrial guidance to the project. All authors contributed
598 to the revision of the study.

599 **Competing interests**

600 The Authors declare no competing interests

601

602 **Figure legends & tables**

603 **Figure 1:** (a) Quinone redox cycling, ROS formation and GSH-based detoxification. A schematic of the single
604 electron reduction of a quinone (Q) to a semiquinone radical anion ($SQ^{\cdot-}$), followed by complete reduction to the
605 hydroquinone (H_2Q). The figure shows the concomitant reduction of molecular oxygen by $SQ^{\cdot-}$ to form the ROS,
606 superoxide ($O_2^{\cdot-}$), followed by its dismutation into hydrogen peroxide (H_2O_2), which is detoxified by glutathione
607 (GSH) into harmless H_2O through the glutathione peroxidase (GPx) reaction. GSH is regenerated from its

608 oxidised form (*GSSG*), catalysed by the glutathione reduction (GR) reaction. Finally, the glutathione-quinone
 609 adduct (*GS-H₂Q*) formation represents the reductive addition (Michael reaction) between GSH and the Q
 610 electrophile. (b) Chemical structure of doxorubicin. The anthracycline contains both the quinone (red) and
 611 hydroquinone (blue) moieties within its chemical structure. The hydroquinone is the site of auto-oxidation for
 612 doxorubicin.

Reaction Rate Equation

R_1	R_1
R_2	$R_2 = k_{p2} [SQ]k_{O2}$
R_3	$R_3 = k_{p3} [SQ]^2$,
R_4	R_4
R_5	$R_5 = k_{p5} [SQ]^2$

613 **Table 1:** Model kinetic expressions. Kinetic terms assembled to describe quinone / doxorubicin redox cycling
 614 are based on the law of mass action. All parameters values were obtained from fitting to experimental data and
 615 are located in the supplementary information. All reactions correspond to Figure 2 only.

616 **Figure 2:** Doxorubicin-quinone redox cycling model schematics. Three variations of quinone redox cycling
 617 (reduced, triad and comproportionation) are described. Each model comprises of a single compartment and a
 618 selection of the following species: quinone (*Q*); semiquinone radical (*SQ[•]*); hydroquinone (*H₂Q*); superoxide
 619 radical (*O₂^{•-}*); molecular oxygen (*O₂*); and hydrogen peroxide (*H₂O₂*). The corresponding reaction rate equations
 620 (R_{1-5}) are described in Table 1.

621 **Figure 3:** Oxygen consumption rate (OCR) profiles for doxorubicin at 50, 37.5, 25, 12.5 and 10 μ M. Each data
 622 point in represents the OCR immediately after a 3-minute solution mix within the well, measured in the transient
 623 microchamber. Compound injection occurs at $t = 16$ min (between measurements 1 and 2). Each dataset is the
 624 average of $n=3$ experiments expressed with its standard deviation.

	Reduced Model	Triad Model	Comproportionation Model
AIC	3.878×10^4	3.239×10^3	3.244×10^3
BIC	3.879×10^4	3.247×10^3	3.253×10^3

625 **Table 2:** AIC and BIC values for the reduced, triad and comproportionation model fits of the OCR data.
626

627 **Figure 4:** Normalised sensitivity measures for the comproportionation model reaction rate constants, expressed
628 as main and total effects.

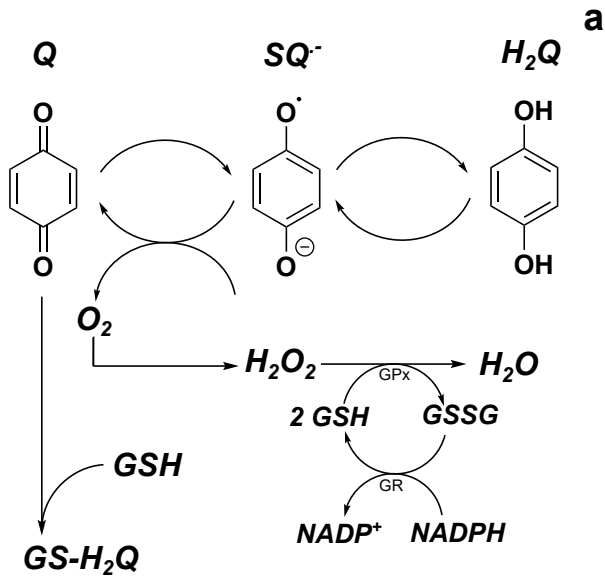
629 **Figure 5:** Triad model fitting and simulation. Comparison of simulated and experimental OCR data for 50, 37.5
630 25 12.5 and 10 μM of doxorubicin (Figure 3).

631 **Figure 6:** Model simulations for doxorubicin and ROS metabolism. The fate of a single doxorubicin exposure
632 (50 μM) was simulated over a 30-minute time-span in order to glean the resulting transformations between Q,
633 SQ^- and H_2Q (top panel). The resulting superoxide and hydrogen peroxide formation and detoxification profiles
634 are illustrated in the bottom left and right panels, respectively.

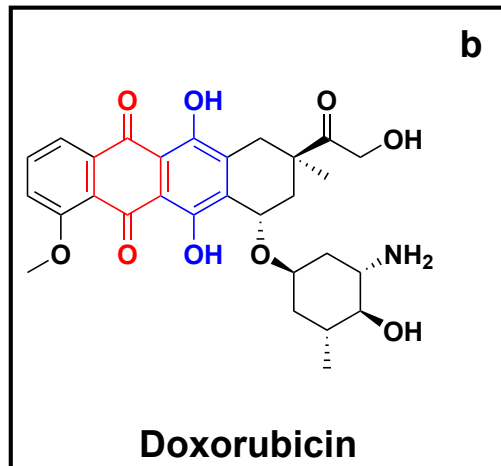
635 **Figure 7:** The effects of doxorubicin quinone-based metabolism on glutathione and cysteine model
636 homeostasis. The resulting simulated changes in blood and cytosolic GSH and cysteine after a single or constant
637 exposure to 50 μM of doxorubicin are shown in A and B respectively, for a 10-hour time-span. % of normal
638 represents the percentage difference of the variable compared to its simulated steady state value.

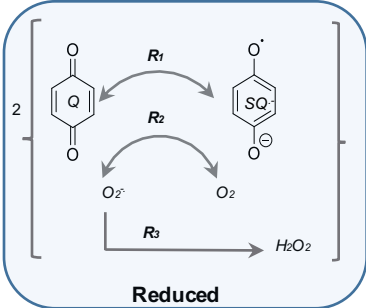
639 **Figure 8:** The effects of doxorubicin quinone-based metabolism on glutathione homeostasis. The resulting
640 simulated changes in cytosolic GSH following single (A) or constant exposure (B) to a range of doxorubicin
641 concentrations (0-50 μM) are shown in A and B respectively, for a 20-hour time-span. The 70% reduction
642 threshold is indicated in (B) with a black dashed line.

643

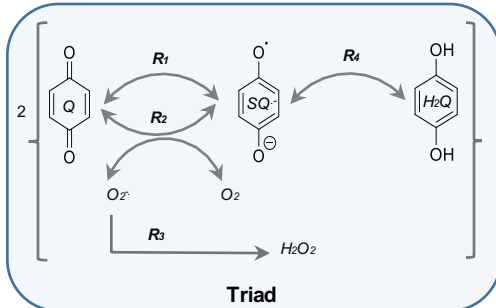


Quinone Redox Metabolism

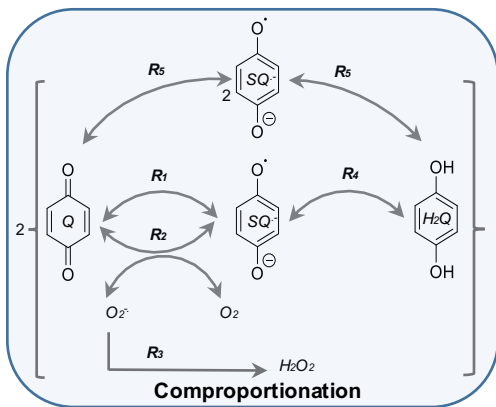




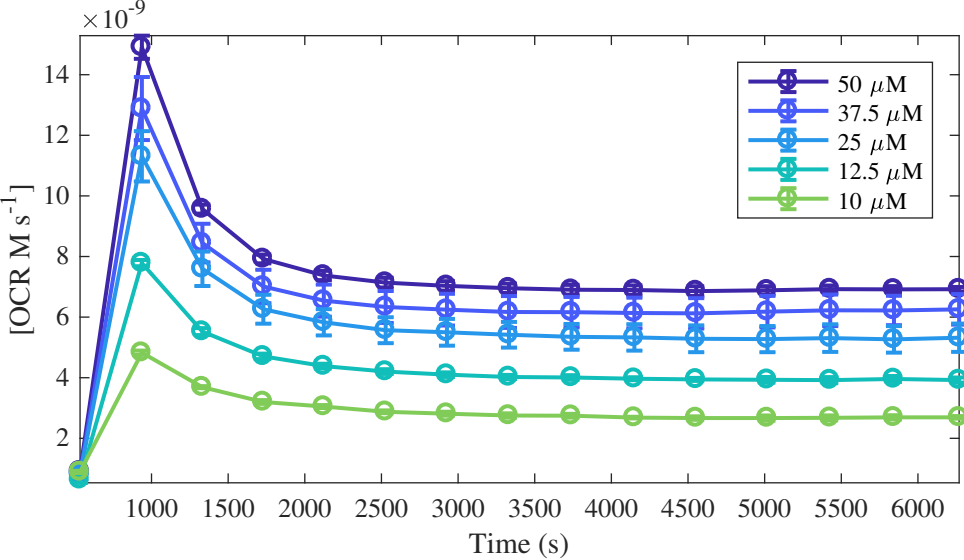
Reduced



Triad



Comproportionation



Normalised Sensitivity Measures

